CLIMATOLOGY OF UPWELLING RELATED PROCESSES OFF BAJA CALIFORNIA

ANDREW BAKUN AND CRAIG S. NELSON

Pacific Environmental Group
Southwest Fisheries Center
National Marine Fisheries Service, NOAA
Monterey, California 93940

ABSTRACT

Marine surface data are used to describe large scale features of upwelling and certain related processes off the west coast of Baja California. The offshore-directed component of sea surface Ekman transport, computed from the wind stress distribution, is considered an index of coastal upwelling intensity. Upwelling appears to be strongest south of 30°N latitude, from March to June. Departures from randomness in the offshore Ekman transport signals include the annual and diurnal periodicities, an energetic irregular rhythm in the "event" frequency range (several day to several week periods), and two types of persistence. A short-term persistence appears to be related to the duration of synoptic scale atmospheric disturbances, while a much longer-term persistence may be related to a feedback mechanism between the upwelling and the overlying wind stress field.

The longshore current field is highly correlated seasonally with the upwelling cycle. Strong equatorward surface flow is indicated during the spring upwelling maximum; during the fall there is generally a poleward component of flow. Wind stress curl distributions indicate a tendency for the surface wind drift to be convergent (negative curl) in the offshore region. From Punta Baja to Punta Eugenia the convergent area extends to the coast. Areas of divergent surface drift (positive curl) extend several hundred kilometers off the coast north of Punta Baja and south of Punta Eugenia. From a "Sverdrup transport" point of view, this pattern is consistent with evidence of separate cyclonic gyral circulations north of Punta Baja and south of Punta Eugenia.

INTRODUCTION

Coastal upwelling is a highly fluctuating process which can have important effects on fishery resources. The role of upwelling in bringing nutrients into the surface layers where they are available for organic production is widely recognized. A related process that may enhance production is the dispersion of grazing organisms by the diverging surface waters, thereby reducing grazing pressure on the phytoplankton stock. In addition to these effects at the very base of the food web, upwelling can alter the temperature distribution, field of motion, stratification, and other characteristics of the physical environment, affecting marine organisms at various levels of their life processes.

At the Pacific Environmental Group we are developing descriptions of upwelling phenomena to aid fishery researchers in accounting for such effects. To be most useful these descriptions should have continuity over the broad space scales and long time scales involved in fishery work. In addition it is desirable that they be continually updated and hindcast over past periods for which knowledge of a fishery is available. Our approach, consequently, has been to avoid basing our work on dedicated observational programs but rather to try to construct a useful descriptive system from observatons routinely reported by ships at sea, weather stations, etc.

Our collocation with the U.S. Navy's Fleet Numerical Weather Central (FNWC) in Monterey, California, provides access to a broad data base including archived historical data, analyzed meteorological products, and real time reports. Several data sources have proven most fruitful. The National Climatic Center's file of marine surface observations has been useful in defining the climatological seasonal cycles. This file contains over 38 million individual ship reports, dating back into the nineteenth century. Similar real-time ship reports continue to be delivered via the international data networks. To describe variations from normal seasonal conditions we have used the analyzed products, notably the surface atmospheric pressure analysis, produced by FNWC. Finally, the U.S. Naval Oceanographic Office ship drift file, which is a compilation from ships' log books of differences between dead reckoning position and accurately detemined position, has been useful as an indication of the seasonal variability of the ocean surface flow field.

Our major focus is the upwelling region off western North America. However, since the data sources are global the methods developed should be applicable to other regions, depending on the density of available data. At this stage much of our work is qualitative. Our goal is to model quantitatively many of the processes which would be useful environmental inputs to fishery management systems for upwelling regions, and to define and develop practical indicator systems to make these inputs operational.

THE SEASONAL CYCLES

To define seasonal variations, long-term composite monthly distributions of various properties were assembled from ship reports contained in the National Climatic Center's file of marine surface

observations (TDF-11). After preliminary gross error checks, similar to those described by Bakun, McLain, and Mayo (1974), climatological scalar properties were compiled by computing the arithmetic means of all available reports within a specified 1-degree square area and long-term (1850–1970) month. Similarly, resultant mean vector quantities have been computed as the arithmetic means by north and east components for all reports in the area. A mean value for any month and square is therefore formed from a data set that is independent of all other months and squares. No attempt has been made to smooth the fields, either by removing data which do not appear to fit the distributions or by applying objective smoothing procedures. The mean values were contoured by machine, and "bulls eyes" in the contours, even where they possibly reflect erroneous data, were left in the figures as indications of the general degree of consistency of the composite fields.

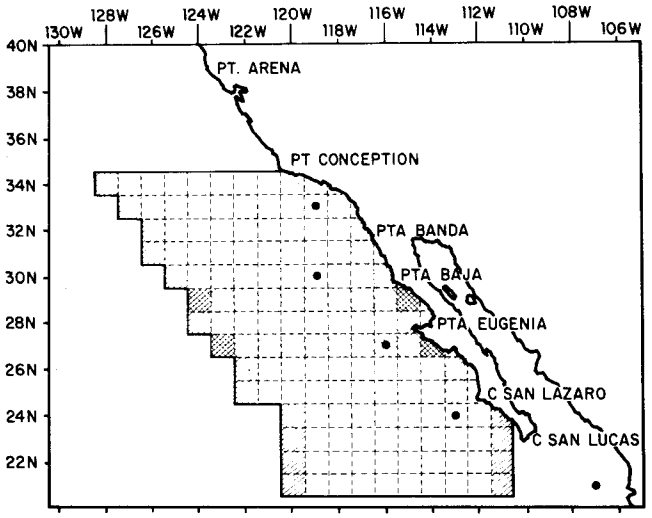

FIGURE 1. Chart of the Baja California region. The grid of 1 degree squares is used for summaries of ship observations. Shading indicates nearshore and offshore lines of selected squares parallel to the coast and lines extending westward from the coast south of Punta Baja and Punta Eugenia used for displays of time-space sections. Large dots indicate 3 degree grid intersections used to compute time series properties.

Approximately 400,000 individual reports are available for the area defined by the grid off southern California and Baja California (Figure 1). The number of reports per 1-degree square per month varies from less than five (in May in the southwest section of the grid), to 3500 (in May off Los Angeles). The spatial distribution of observations is biased in that "ship of opportunity" reports are generally confined to coastwise shipping lanes. The highest density of reports is found within 3 degrees of the coast and north of 30°N latitude. Significant temporal bias may exist, since approximately 50% of the total available observations have been taken since 1945. Nevertheless, the coherence of the resulting vector and scalar fields indicates that our composite distributions can be used to describe the dominant seasonal cycles in upwelling related processes. Moreover, comparisons between our monthly sea surface temperature fields and those of Robinson and Bauer (1971), for example, show good correlation.

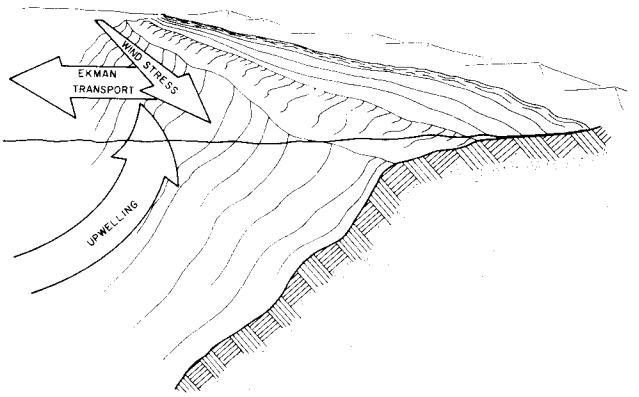

FIGURE 2. A conceptual diagram of the coastal upwelling process. The coast of the continent is represented in cutaway view with the ocean to the left of the figure. Offshore transport in the surface Ekman layer of the ocean due to stress of the wind is replaced by upwelling from depth.

In a simplified view of the coastal upwelling process, equatorward wind stress parallel to the coast induces flow in the surface layers of the ocean which is deflected offshore by the earth's rotation (Figure 2). When this occurs over a wide expanse of coast where longshore horizontal surface flow cannot compensate for that driven offshore, the balance is maintained by upwelling of deeper water. Wooster and Reid (1963) approximated the wind-driven offshore flow as Ekman transport and showed that this "index of upwelling" explained in general the observed features of coastal upwelling in broad diffuse eastern boundary currents such as exists off Baja California.

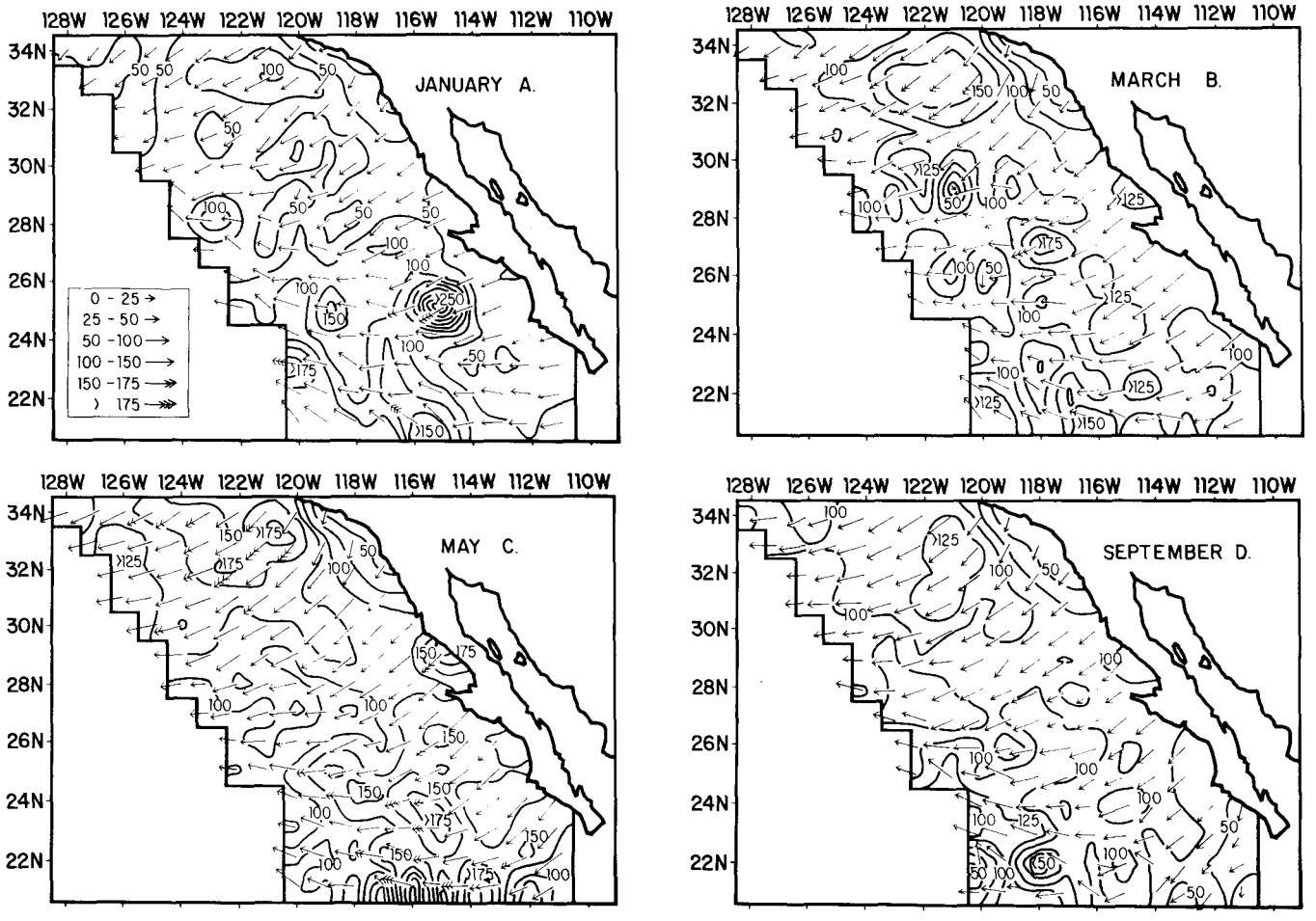

FIGURE 3. Sea surface wind stress. Monthly composite fields of resultant vectors were summarized by 1 degree squares from historical ship observations for A. JANUARY, B. MARCH, C. MAY, and D. SEPTEMBER. Units are dynes/cm². Magnitudes are contoured at intervals of 0.5 dynes/cm². Vector symbols are scaled according to the key.

Wind Stress

In producing the long term composite monthly sea surface wind-stress distributions (Figure 3), the stress was calculated from each wind velocity report according to

$$\tau = \rho_a \, C_D \, |\vec{v}| \, \vec{v} \qquad (1)$$

where:

$\vec{\tau}$ denotes the stress vector

ρ_a is the density of air which was considered to have a constant value of 0.00122 g/cm³

$|\vec{v}|$ is the observed wind speed

$\vec{v}$ is the observed wind velocity vector

C_D is an empirical drag coefficient.

A constant drag coefficient of 0.0016 (Denman and Miyake, 1973) was employed.

The fields show the tendency for an equatorward component of stress to parallel the coast of Baja California, which implies conditions favorable for upwelling throughout the year. Most of the seasonal variability appears in magnitude rather than in direction. A wind stress maximum appears south of Point Conception in March. During May (Figure 3C), stress exceeds 1.0 dyne/cm² within the region north of 30°N latitude, while values for most of the offshore region to the south lie between 0.5 and 1.0 dyne/cm². The maximum immediately north of Punta Eugenia is a consistent feature during the spring. The mean distributions for January and September (Figures 3A and 3D) indicate relaxed conditions. Typical values of surface stress are less than 0.5 dyne/cm². A region of minimum wind stress is indicated along the coast from Point Conception to Punta Banda. This feature corresponds in location to the cyclonic eddy which dominates the ocean surface circulation in the Southern California Bight (Reid, Roden, and Wyllie, 1958).

Surface Wind Transport

Our estimates of the transport in the surface layer of the ocean due to the stress of the wind are based on Ekman's (1905) theory which leads to the following equation for the total integrated mass transport of pure drift currents:

$$\vec{V}_E = \frac{1}{f\rho} \vec{\tau} \times \vec{k} \qquad (2)$$

where:

$\vec{V}_E$ is the total mass transport resulting from an applied local wind stress

f is the Coriolis parameter

$\vec{k}$ is a unit vector directed vertically upward

corresponding increases in the computed Ekman transport. Offshore gradients in the surface transport may contribute to convergences and divergences,

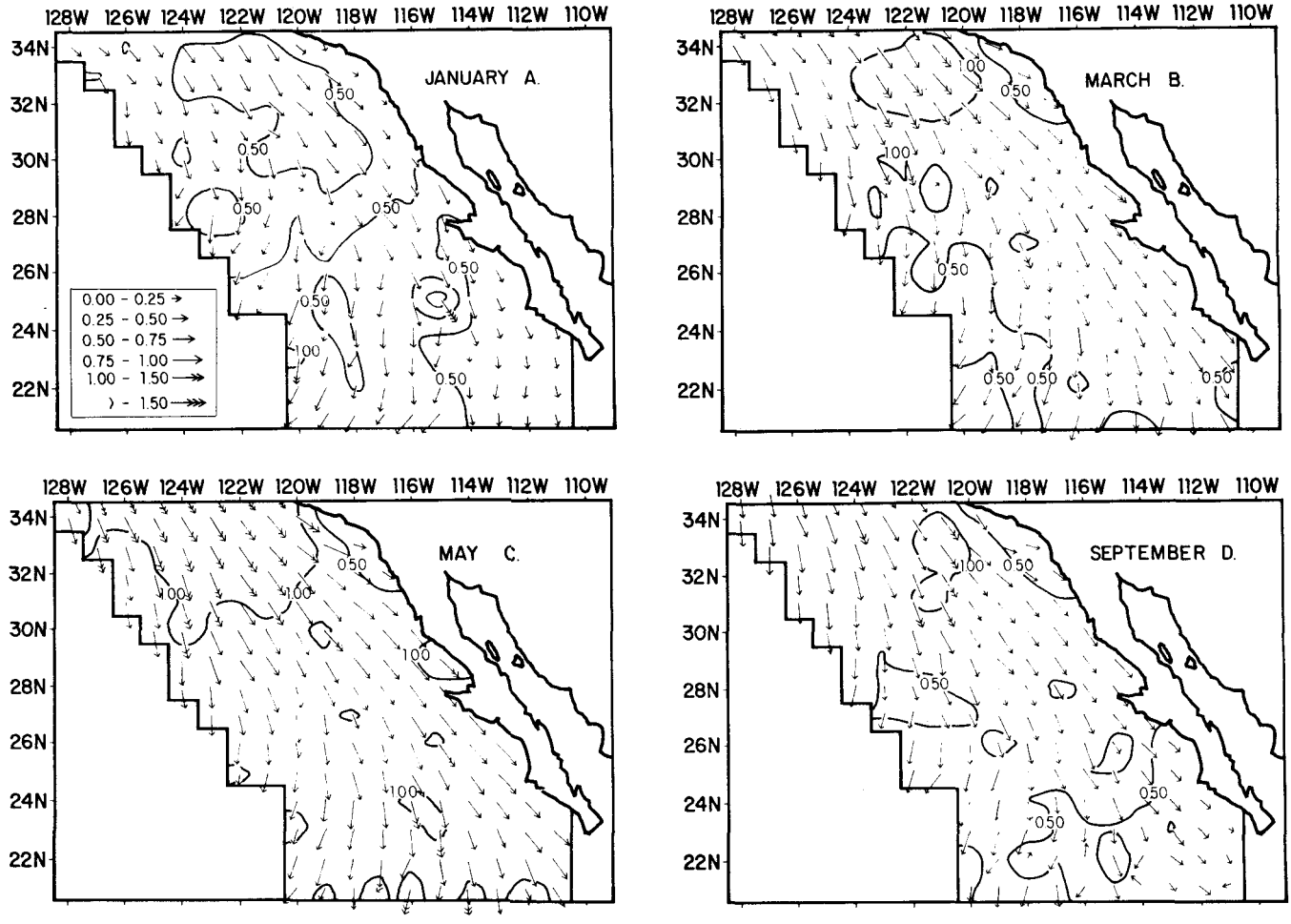

FIGURE 4. Surface Ekman transport. Monthly composite fields of resultant vectors were summarized by 1 degree squares from historical ship observations for A. JANUARY, B. MARCH, C. MAY, and D. SEPTEMBER. Units are metric tons per second per 100 meters coastline. Magnitudes are contoured at intervals of 25 units. Vectors symbols are scaled according to the key.

The relationship implies that the integrated transport is directed 90° to the right of the wind stress in the northern hemisphere.

Composite monthly fields of Ekman transport (Figure 4) were calculated by applying equation (2) to the mean distributions of surface wind stress. The mean transport is directed offshore throughout the year. Accordingly, our conceptual model (Figure 2) indicates strong upwelling in regions of coastal divergence in March and May (Figures 4B and 4C). During these months local maxima in the surface transport appear north of 30°N latitude, immediately north of Punta Eugenia, and south of 24°N, where the decrease in the Coriolis parameter leads to thereby altering the distributions of organisms.

The seasonal cycle of Ekman transport (Figures 5 and 6) within the selected 1-degree squares adjacent to the coast (Figure 1) indicates the general seasonal pattern of local wind forcing of coastal upwelling. The degree of correspondence in general shape and position of the contours of absolute magnitude in the vector time series (Figure 5) with the contours of magnitude of the offshore component (Figure 6) illustrates the primarily offshore direction of wind driven surface flow off Baja California, implying some degree of upwelling on average throughout the year. Strongest upwelling appears to occur from March to June, and along the coast from 20°N to 30°N.

A maximum is apparent north of Punta Eugenia at 28°N latitude. From September to December, offshore transport weakens, and changes sign in September at 21°N. July and August, and January and February appear to be transition periods.

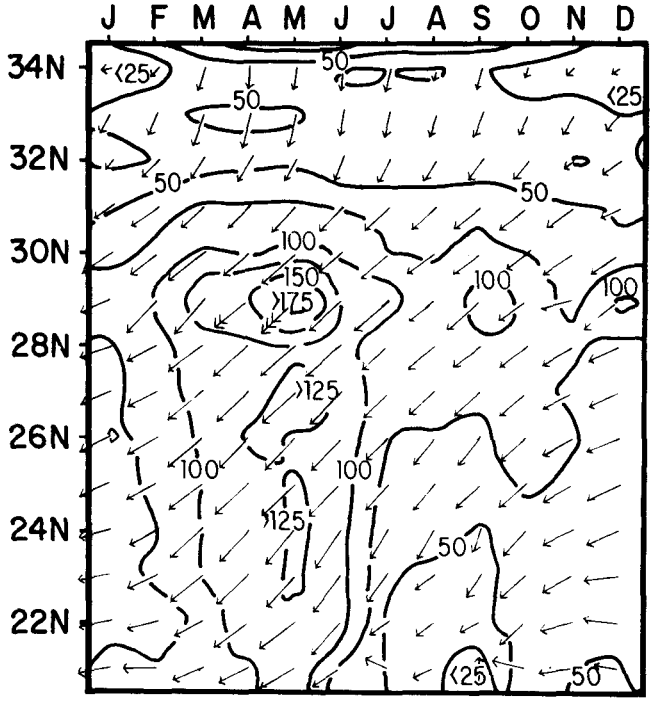

FIGURE 5. Seasonal cycle of Ekman transport near the coast. Resultant vectors were summarized by month for the group of selected 1 degree squares adjacent to the coast shown in Figure 1. Units are metric tons per second per 100 m coastline. Magnitudes are contoured at intervals of 25 units. Vector symbols are scaled according to the key in Figure 4A.

In addition to the surface Ekman wind drift, the ocean surface flow field also contains geostrophic components. Sverdrup, Johnson, and Fleming (1942, page 501) describe a linkage by which the accumulation of denser upwelled water near the coast and the transport away from the coast of lighter surface water leads to a redistribution of mass. The balance between the resulting pressure gradient and the Coriolis force produces a geostrophic current in the equilibrium state. Consequently, on a seasonal basis, one might expect variations in the offshore component of Ekman transport to be well correlated with variations in longshore flow. Indeed, investigators in CUEA have demonstrated this correspondence on shorter time scales (Huyer, et al., 1974).

Surface Currents

The only available direct measurements of ocean surface flow having reasonable spatial and seasonal coverage are reports of drift attributed to ocean currents, compiled from ships' log books. We have made seasonal summaries from the ship drift file of

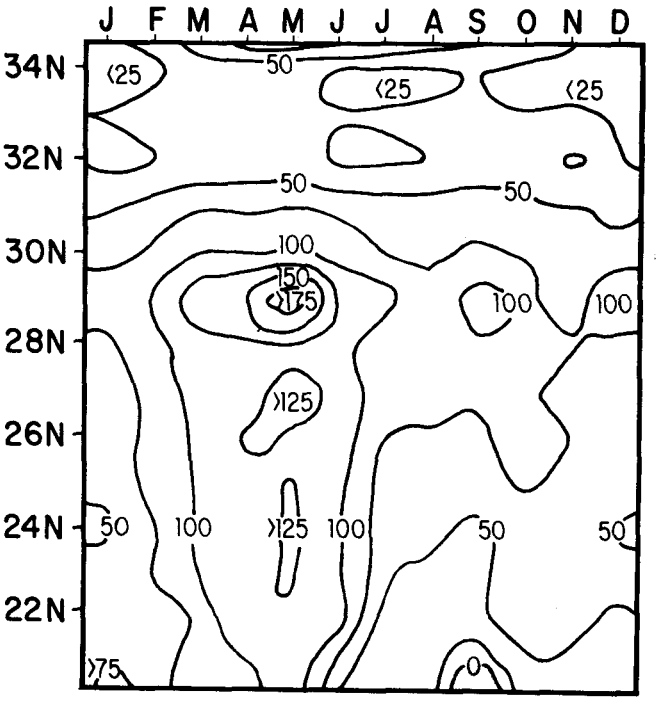

FIGURE 6. Seasonal cycle of offshore Ekman transport. Means of offshore components of Ekman transport were computed by month within the group of selected 1 degree squares near the coast shown in Figure 1. Units are metric tons per second per 100m coastline. Onshore Ekman transport is shaded.

the U.S. Naval Oceanographic Office. These data are much the same as used by Wyrtki (1965). The density of available reports is only about one-tenth that of marine surface observations and is dependent upon the primary coastwise shipping lanes. Significant bias by month and year is apparent; March, May, and November contain approximately two to four times as many observations as any other month, and most of the observations were reported prior to 1940.

Ship drift distributions are inherently noisy and require a large data base to resolve the underlying patterns. To increase the number of observations per averaged value, we have used summaries by 2-degree squares, by month (Figures 7 and 8), and by quarter (Figure 9). The precise interpretation of these measurements remains open to question since wind effects on reporting vessles are indeterminate. However, Stidd (1974) has indicated a closer correspondence of ship drift to ocean current direction than to wind direction. In addition, mean ship drift vectors are in some cases directed oppositely to mean wind vectors. The Southern California Countercurrent is an example.

A significant correlation between the longshore component of surface current (Figure 8) and the offshore component of Ekman transport (Figure 6) is apparent. Specifically, during the period of maximum offshore transport, equatorward surface flow in the California Current is strongest. Indeed, there is a correspondence between the position of

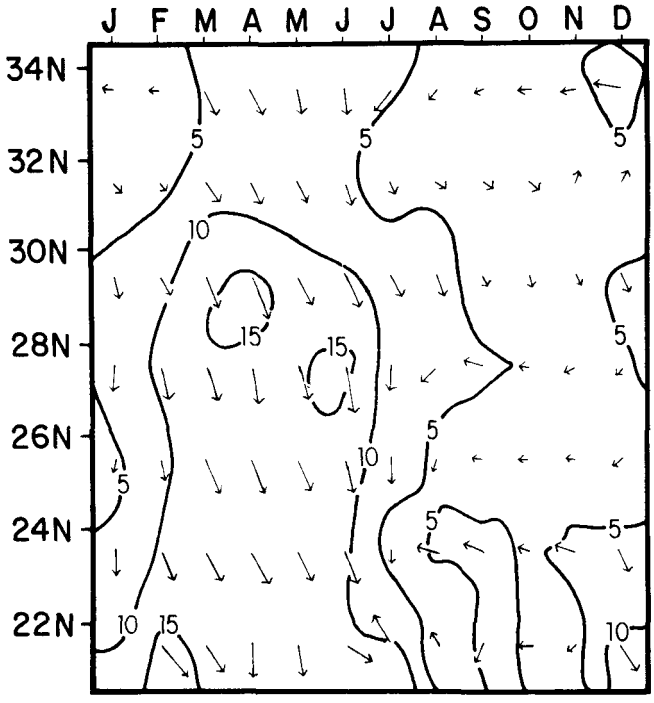

FIGURE 7. Seasonal cycle of ship drift near the coast. Resultant vector were summarized by month from the NAVOCEANO ship drift file, for a group of 2 degree squares along the coast from latitude 20°N to 34°N. Units are cm/sec. Magnitudes are contoured at intervals of 5 cm/sec. Vector symbols are scaled according to the key in Figure 9A.

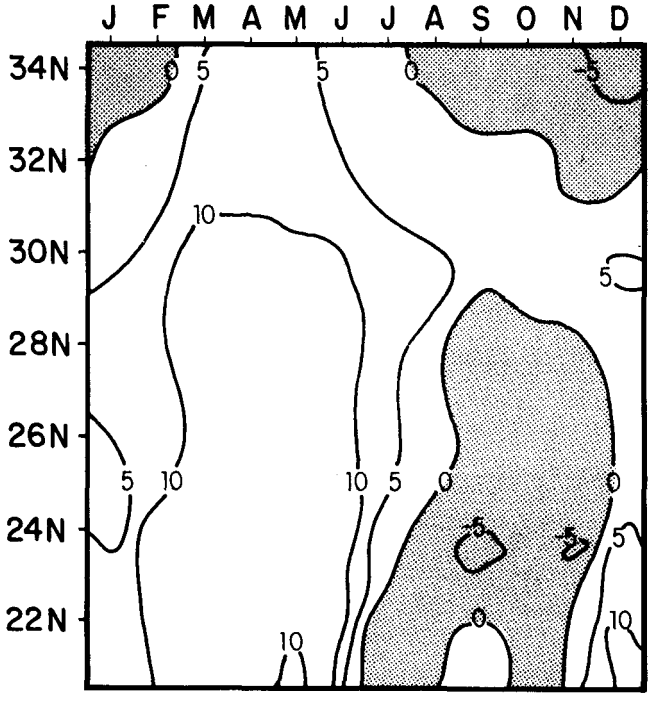

FIGURE 8. Seasonal cycle of longshore ship drift. Means of components parallel to the coast were summarized from the NAVOCEANO ship drift file for a group of 2 degree squares along the coast from latitude 20°N to 34°N. Units are cm/sec. Positive values indicate equatorward drift. Poleward drift is shaded.

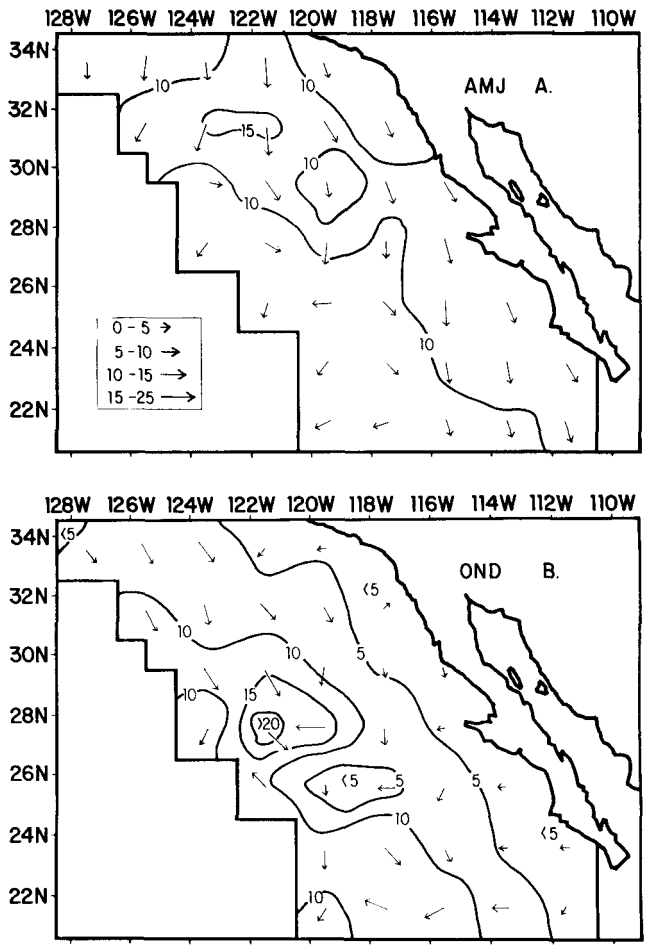

FIGURE 9. Ship drift. Composite field of resultant vectors were summarized by quarter and by 2 degree squares from the NAVOCEANO ship drift file for A. APRIL-MAY-JUNE and B. OCTOBER-NOVEMBER-DECEMBER. Units are cm/sec. Magnitudes are contoured at intervals of 5 cm/sec. Vector symbols are scaled according to the key.

the maximum offshore Ekman transport north of Punta Eugenia (Figure 5) and the position of the strongest longshore surface currents at latitude 29° N in April and May (Figure 7). During the relaxed period of upwelling, from September to December, the surface current changes direction and flows offshore, but has a definite poleward component along the coast. The surface current data indicate cyclonic flow in the Southern California Bight, where offshore Ekman transport is less than 50 metric tons per second per 100 m of coastline throughout the year. These data suggest that the surface countercurrent off Baja California may only form where offshore Ekman transport is weak.

During the spring upwelling season, surface current parallels the coast with only a slight offshore component (Figure 9A) and reaches a maximum strength of about 15cm/sec (Figure 7). During the period of relaxed upwelling, the current changes direction and slows to less than 5 cm/sec (Figure 9B). Flow is primarily offshore, but there is some

suggestion of a coastal countercurrent. The lack of coherence in the distributions between 7 and 10 degrees off the coast reflects scarcity of data.

Sea Surface Temperature

Vertical and horizontal advection associated with coastal upwelling alter the patterns of surface isotherms which are approximately zonally distributed off Baja California. The composite surface temperature field for June (Figure 10) shows cold water indicative of upwelling along the coast from Punta Eugenia to Punta Baja. This feature correlates well with the local Ekman transport maximum in the same area. South of latitude 25° N, indications of upwelling in the temperature distribution are slight. In the region off southern California, the warm coastal temperatures may reflect seasonal heating and warm advection in the cyclonic eddy (Reid, Roden, and Wyllie, 1958).

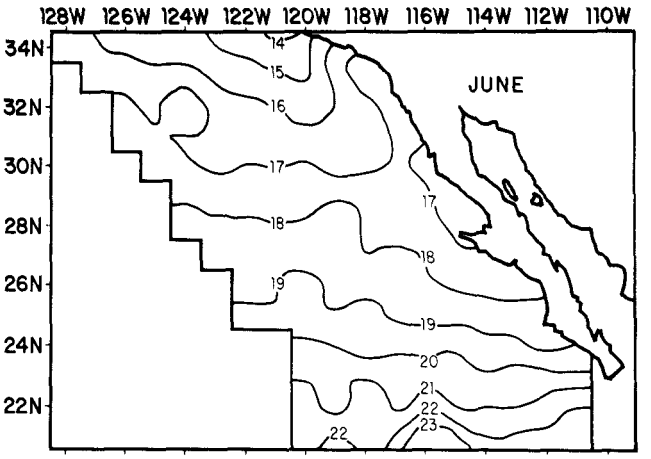

FIGURE 10. Sea surface temperature during June. Mean values of sea surface temperature observations were computed by 1 degree squares for the month of June. Units are degrees Celsius.

The coarse resolution in the 1-degree spatial summaries used in this paper tends to mask fine scale features of the temperature distributions. These particular temperature fields were developed to be compatible in resolution to, and used in conjunction with, our other data fields. More detailed treatments can be found in California Marine Research Committee (1963), Lynn (1967), and Wyllie and Lynn (1971).

The seasonal cycle of the sea surface temperature offshore (Figure 11) shows a normal north-south temperature gradient and a seasonal warming-cooling cycle with a typical range of 2° C to 4° C. Minima occur from February to March and maxima from August to September.

Comparison of the temperature cycle near the coast (Figure 12) with that occurring offshore (Figure 11) shows differences which may be largely

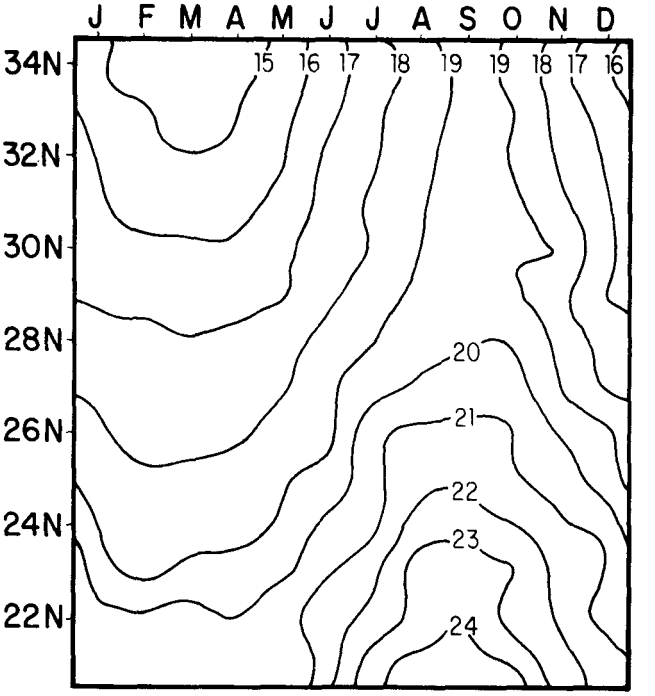

FIGURE 11. Seasonal cycle of sea surface temperature in the offshore region. Mean values of sea surface temperature observations were computed by month for the group of selected 1 degree squares indicated in Figure 1 at the offshore edge of the grid. Units are degrees Celsius.

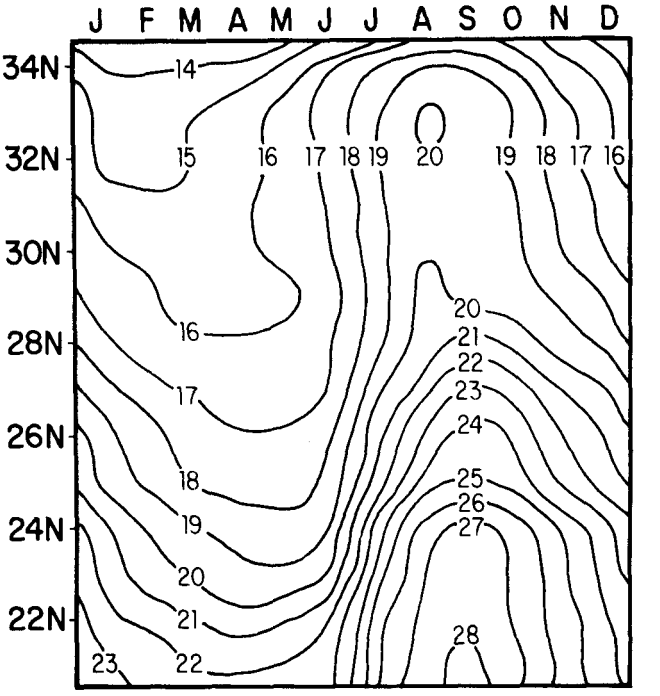

FIGURE 12. Seasonal cycle of sea surface temperature near the coast. Mean values of sea surface temperature observations were computed by month for the group of selected 1 degree squares adjacent to the coast, indicated in Figure 1. Units are degrees Celsius.

attributable to the effect of coastal upwelling, and to differences between horizontal advection in the offshore region and that in the coastal region. There is also the possibility of significant spatial differences in ocean-atmosphere heat exchange. Near the coast the seasonal temperature minimum is delayed relative to that offshore, occurring from March to May in phase with the maximum offshore Ekman transport. A more rapid increase of temperature near the coast during early summer, corresponding to the weakening of the southward surface flow (Figure 7), leads to significantly higher temperatures near the coast during summer than at the same latitude offshore.

Time series displays of seasonal sea surface temperatures in lines of squares extending westward from the coast (Figures 13 and 14) show colder water appearing near the coast in March. The gradients extend several hundred kilometers offshore during spring. During early summer, advection and possible spatial variations in ocean-atmosphere heat exchange processes offset the upwelling indicated by a continued, although weakened, offshore Ekman transport (Figure 6), leading to nearly homogeneous temperatures in the offshore direction. By late summer, warmer advection near the coast relative to that occurring offshore appears to dominate. Warm temperatures are found near the coast; gradients extend hundreds of kilometers offshore. During late fall and winter southward flow begins to increase (Figure 8) and the offshore temperature distribution again becomes nearly homogeneous (Figures 13 and 14).

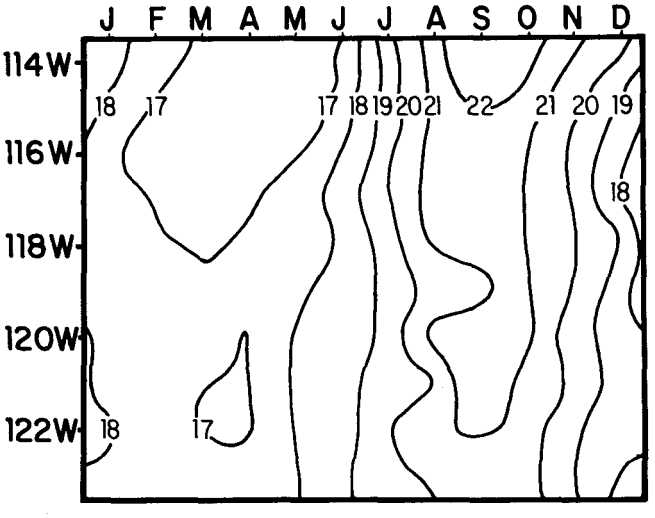

FIGURE 13. Seasonal cycle of sea surface temperature off Punta Eugenia. Mean values of sea surface temperature observations were computed by month for the group of selected 1 degree squares extending westward from the coast south of Punta Eugenia, indicated in Figure 1. Units are degrees Celsius.

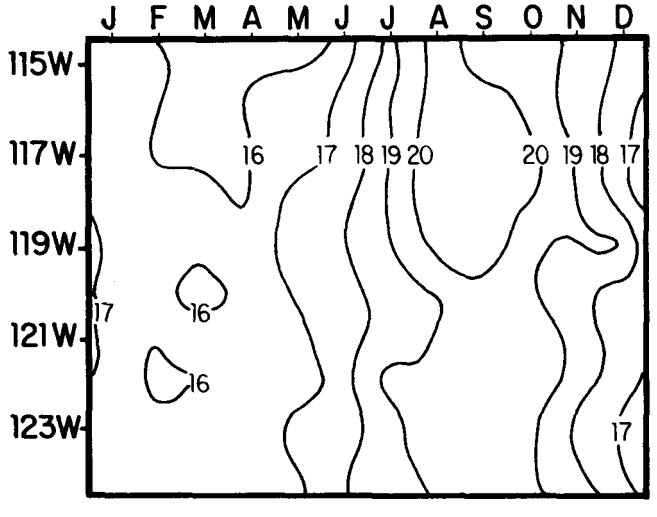

FIGURE 14. Seasonal cycle of sea surface temperature off Punta Baja. Mean values of sea surface temperature observations were computed by month for the group of selected 1 degree squares extending westward from the coast south of Punta Baja, indicated in Figure 1. Units are degrees Celsius.

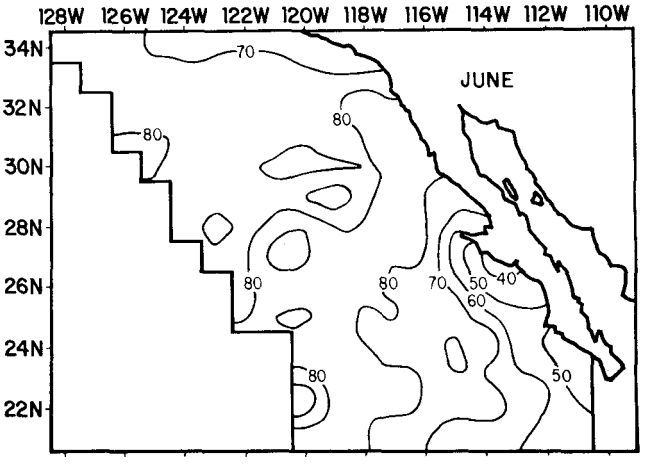

FIGURE 15. Cloud cover during June. Means of reported cloud amounts were computed by 1 degree squares during the month of June. Units are percent of sky obscured.

Cloud Cover

Seasonal and spatial variations in the heat exchange may mask features of upwelling normally evident in distributions of sea surface temperature. In the composite field of total cloud cover for June (Figure 15), Punta Eugenia separates an area of minimum cloud cover along the coast (less than 50%), from an area of maximum cloud cover (greater than 80%). A change in total cloud cover from 40% to 80% could result in a relative decrease of more than 30% in the incident radiation (Seckel and Beaudry, 1973) with corresponding changes in the sea surface temperature.

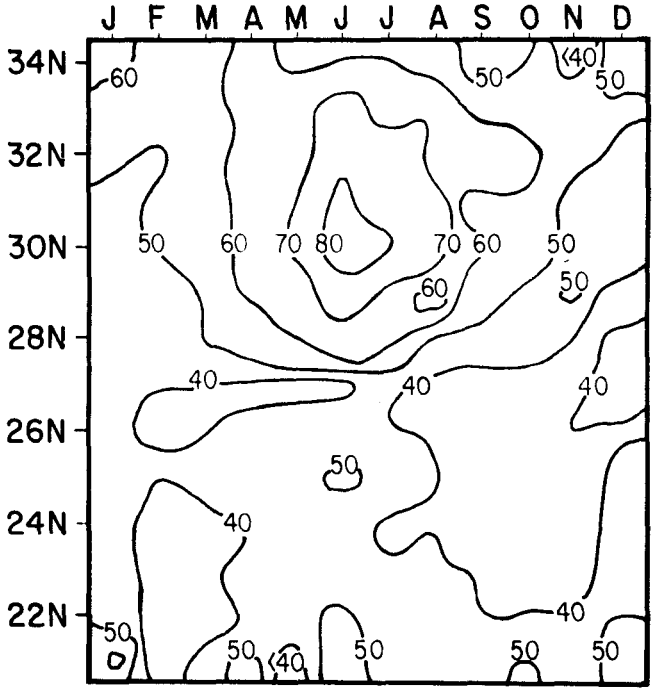

FIGURE 16. Seasonal cycle of cloud cover near the coast. Mean values of reported cloud amounts were computed by month for the group of selected 1 degree squares adjacent to the coast, indicated in Figure 1. Units are percent of sky obscured.

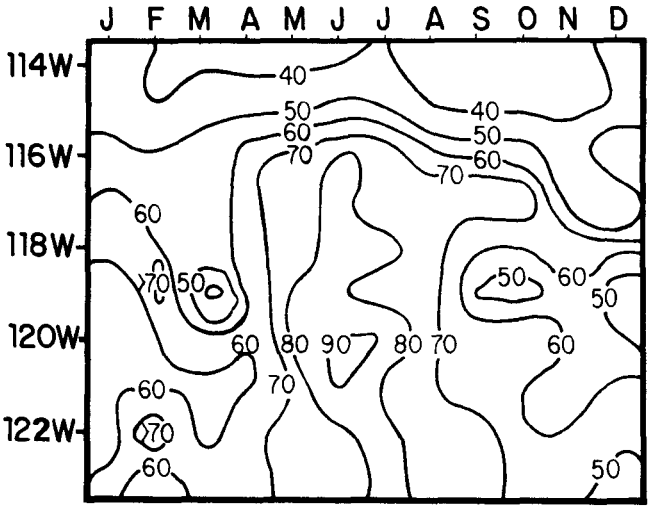

FIGURE 17. Seasonal cycle of cloud cover off Punta Eugenia. Mean values of cloud cover observations were computed by month for the group of selected 1 degree squares extending westward from the coast south of Punta Eugenia, indicated in Figure 1. Units are percent of sky obscured.

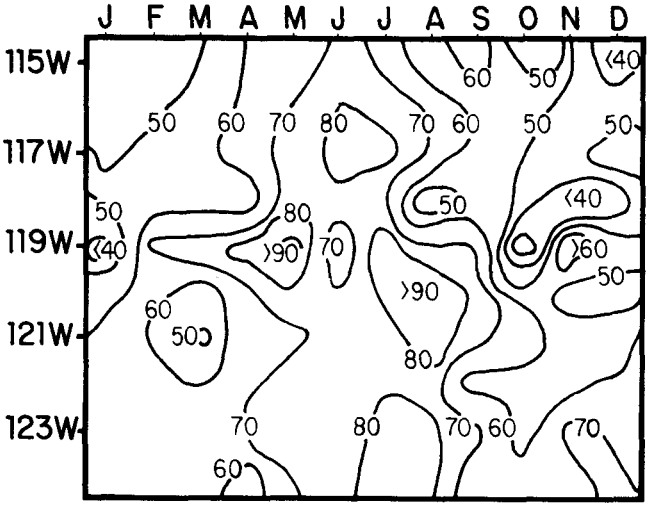

FIGURE 18. Seasonal cycle of cloud cover off Punta Baja. Mean values of cloud cover observations were computed by month for the group of selected 1 degree squares extending westward from the coast south of Punta Baja, indicated in Figure 1. Units are percent of sky obscured.

Considering the seasonal variations in cloud cover within the longshore section of coastal squares (Figure 16), maximum cloud cover appears to be associated with the upwelling off Punta Baja, while minimum cloud cover is evident along the entire coast south of Punta Eugenia. When distributions of cloud cover for sections extending westward from the coast are considered (Figures 17 and 18), the section off Punta Eugenia indicates minimum cloud cover at the coast throughout the year, while relative maxima occur at the coast in the Punta Baja section during June and July. The data suggest that differences in the downward flux of radiation associated with these cloud cover distributions could lessen the indications of coastal upwelling in the sea temperature south of Punta Eugenia. To the north, however, the heat flux from the atmosphere during the upwelling season may be insufficient to obscure the effects of cold water upwelled into the surface layer.

Wind Stress Curl

Although coastal upwelling occurs only at the ocean boundary, wind-induced upwelling can occur whenever divergence in the surface wind drift is not compensated by other modes of horizontal surface flow. The divergent or convergent nature of the surface Ekman wind drift offshore of the primary coastal upwelling zones is determined by the wind stress curl (Figure 19). If the equatorward wind stress parallel to the coast increases in the offshore direction, a situation characterized by positive curl in the stress field, the offshore component of Ekman transport likewise increases in the offshore direction. The result is continued divergence offshore requiring upwelling to maintain the mass balance. Conversely, if the equatorward longshore wind stress decreases in the offshore direction, the wind stress curl is negative. The result is convergence in the surface wind drift with corresponding frontal formation and downwelling.

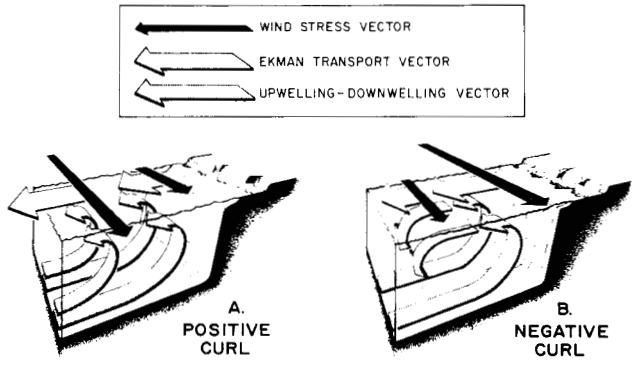

FIGURE 19. A conceptual diagram of the relationship of wind stress curl to divergence and convergence of surface Ekman transport offshore of the primary coastal upwelling zone. An increase in the equatorward wind stress parallel to the coast (positive wind stress curl) produces divergence in surface Ekman transport and continued upwelling offshore. A decrease in the equatorward wind stress parallel to the coast (negative wind stress curl) produces convergence in surface Ekman transport and downwelling offshore.

Actual observations of wind stress curl are not available. Alternatively, we have computed the curl of the mean wind stress fields under the assumption that, since the curl is a linear operator, the resulting distributions may resemble mean fields of actual wind stress curl distributions existing off Baja California. Monthly curl fields corresponding to the mean wind stress distributions (Figure 3) were determined (Figure 20). Negative wind stress curl (Ekman convergence) is characteristic of the offshore region. From Punta Baja to Punta Eugenia the convergent region reaches to the coast. The wind stress distributions thus imply favorable conditions for formation of fronts and convergent patches of recently upwelled water in this area. North of Punta Baja and south of Punta Eugenia areas of positive curl (Ekman divergence) extend from the coast to several hundred kilometers seaward. Within these divergent areas there would tend to be a continued, although much reduced, level of upwelling offshore of the primary coastal upwelling zone.

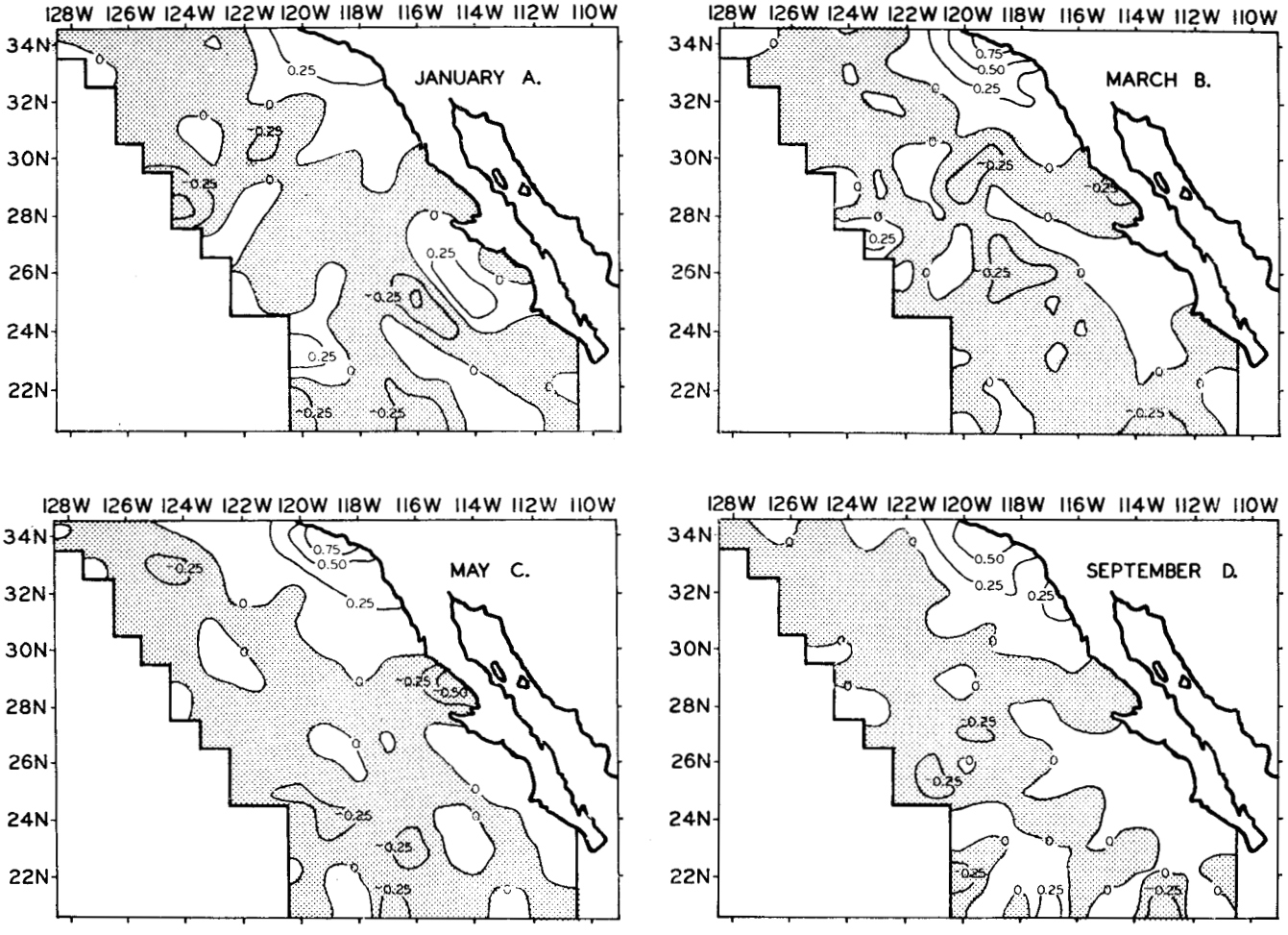

FIGURE 20. Wind stress curl. Monthly composite fields of wind stress curl were computed from the surface wind stress fields shown in Figure 3; A. JANUARY, B. MARCH, C. MAY, and D. SEPTEMBER. Units are dynes/cm²/100km. The coutour interval is 0.25 dynes/cm²/100 km. Negative values are shaded.

Munk (1950) has suggested that the poleward undercurrent observed along the California coast may be a consequence of the local wind stress curl. Pedlosky (1974) has indicated theoretically that a poleward undercurrent would be favored by positive wind stress curl along the coast and a poleward decrease in the surface heating. The surface data presented here cannot describe features of the subsurface flow. However the mean wind stress distributions off the coast appear generally consistent with a pattern of countercurrent inshore and equatorward flow offshore, except in the region from Punta Eugenia to Punta Baja where the wind stress curl is not positive. During the fall, the relaxation of upwelling induced equatorward surface flow would favor surfacing of a coastal countercurrent. With these considerations in mind it is interesting to note that indications of a poleward component of ship drift during fall (Figure 9B) are lacking in the region from Punta Eugenia to Punta Baja. Rather, the data suggest separate cyclonic gyres in the regions of positive wind stress curl off the Los Angeles Bight and south of Punta Eugenia.

VARIABILITY AND PERSISTENCE

In addition to responding to the seasonal variations, marine biological communities must also respond to a wide spectrum of environmental variations of time scales ranging from many years to small fractions of a year. A central problem in investigating such fluctuations is the formation of consistent time series of pertinent information.

For any particular synoptic sampling the available reports from ships at sea tend to be sparse and unevenly distributed. In such a situation the variability introduced by random errors in measurement or changes in spatial distribution of reports may be as great or greater than the variability in the process itself. If a definite periodicity is known it may be reasonable to composite corresponding portions of different cycles, as was done in the previous section, in order to obtain an adequate data base. This is not possible in the case of fluctuations which are nonperiodic or where, if they do contain periodic components, the periodicities are undefined.

One way to arrive at fairly consistent time series of wind information with which to investigate fluctuations in upwelling is to make use of analyzed products produced by meteorological agencies. In this section we use 6-hourly computations of offshore Ekman transport based on the synoptic surface atmospheric pressure analyses produced by Fleet Numerical Weather Central. These analyses incorporate all available wind reports in the form of equivalent pressure gradients as well as the available pressure data (Holl and Mendenhall, 1972). Conventional reporting periods correspond to 4AM, 10AM, 4PM, and 10PM Pacific Standard time, yielding four synoptic samplings per day.

Bakun (1973) described a procedure for computing offshore Ekman transport from pressure fields using a geostrophic wind computation and a simplified boundary layer approximation. The results of such computations were called *upwelling indices.* A compilation of daily and weekly means of 6 hourly indices at 15 locations off western North America has been published (Bakun, 1975). The time series discussed in this paper are located at five 3 degree grid intersections, from 21°N to 33°N latitude (Figure 1).

This 3 degree resolution is coarse compared to the 1 degree resolution achieved in the previous section. The pressure fields were originally analyzed on a grid of approximately 3 degree mesh length. Thus any information derived on a smaller scale would consist merely of the details of the particular interpolation function used, rather than having any basis in observed data. Underlying this situation is the fact that the number of reports from the area off Baja California during any synoptic period is only of the order of one per 3 degree square and so analysis of pressure on a smaller scale grid would not increase the resolution of data-based information.

The drag coefficient used in equation (1) to compute these indices was 1.3×10^{-3}. This differs from the value 1.6×10^{-3}, based on the work of Denman and Miyake (1973), used in the previous section. Recent progress in the field of ocean-atmosphere boundary processes suggests that 1.3×10^{-3} may be a more appropriate constant value.

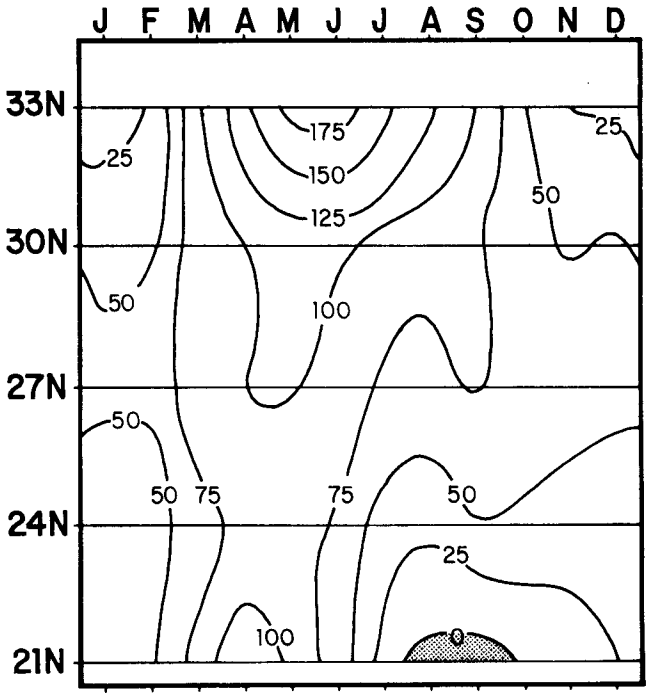

FIGURE 21. Mean values by month and position of 6 hourly coastal upwelling indices for the 7 year period, 1967–73. Locations are indicated by large dots in Figure 1. Units are m^3 per second per 100 m of coast. Negative values are shaded.

Actually the drag coefficient appears to vary both with atmospheric stability and with spectral properties of the ocean waves (Davidson, 1974), but the form of the dependencies does not appear well enough established to warrant incorporation of these effects for our purposes. Since the drag coefficient enters linearly into the computations of stress and Ekman transport, the values in the previous section could be adjusted to those of this section by multiplication by the factor $1.3/1.6 = 0.8125$. Because of such uncertainties, these results, although yielding reasonably realistic numerical values, should properly be viewed as being "uncalibrated" in terms of absolute quantitative detail. The uncertainty in magnitudes is more severe in the case of indices computed from analyzed pressure fields.

Comparison of the 7 year (1967–73) mean values of the 6 hourly upwelling indices (Figure 21) to the seasonal cycle of offshore Ekman transport composited on a 1 degree basis from actual ship reports (Figure 6) illustrates the smoothing of gradients and other spatial details on the 3 degree synoptic index format. It also illustrates a severe spatial distortion in absolute magnitudes discussed by Bakun (1973) which results in amplification of the computed indices at 33°N latitude relative to those at points further south. The figures in this paper which display absolute magnitudes of computed upwelling indices are intended to indicate temporal variations, i.e. relationships along the horizontal axis of the figures. Contours are connected between different locations only as a visual aid and to indicate variations in seasonal timing between different locations. Comparisons of absolute magnitudes on the vertical axis can be misleading. In the case of normalized properties such as skewness and kurtosis the problem is less severe.

Properties of Fluctuations

High variance in the 6-hourly computed indices tends generally to correspond in season and location to high mean value (Figure 22). Thus the winter season is characterized by a generally relaxed level of activity and thus a more stable upwelling regime. Two variations from the pattern are noticeable. At 21°N latitude where during late summer the mean goes negative, i.e. downwelling occurs on average, there is a relative maximum in the variance. Thus the low mean absolute values must reflect a near cancellation of contributions to the variance by large positive and negative fluctuations. Off central Baja California where there are double peaks in the mean, the larger occurring in spring and the lesser in late summer, the late summer period exhibits the greater variance.

Skewness of the monthly distributions is generally positive (Figure 23). Thus the strong departures from the mean are most often spikes of even more intense upwelling separated by longer relaxed periods rather than an equal mix of fluctuations above and below the norm. Highly skewed distributions are at 21°N latitude during the spring

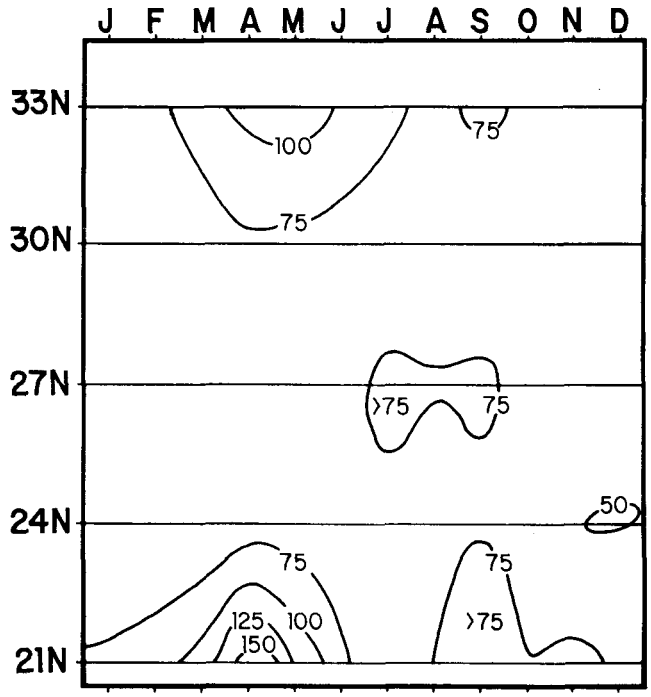

FIGURE 22. Standard deviations of monthly distributions of 6 hourly coastal upwelling indices. Locations are indicated by large dots in Figure 1. Units are m^3 per second per 100 m of coast. Period covered is 1967–73.

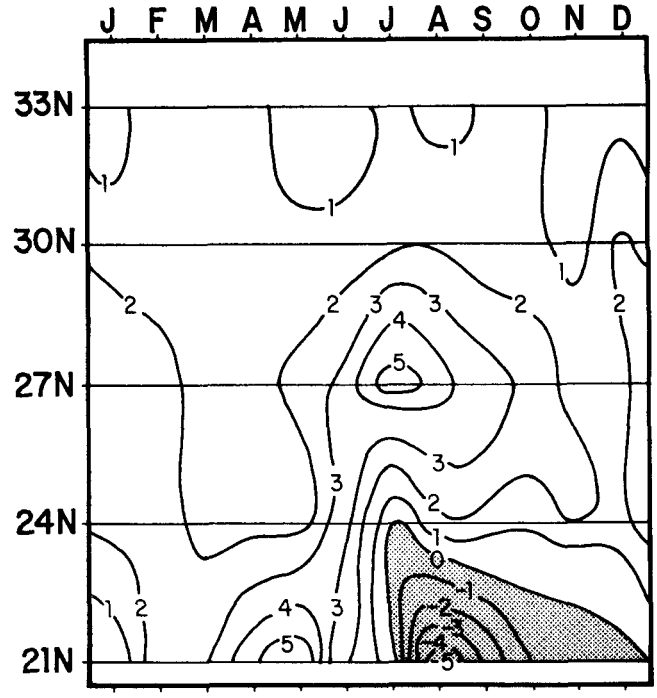

FIGURE 23. Skewness of monthly distributions of 6 hourly coastal upwelling indices. Locations are indicated by large dots in Figure 1. Period covered is 1967–73. Negative values are shaded.

upwelling maximum and off Central Baja California during the relative minimum which separates the spring and late summer maxima. The skewness turns negative during late summer and fall at 21°N. The area of negative skewness extends to 24°N during July and corresponds to a similarly shaped region of low mean monthly values of the indices (Figure 21). This situation appears to be one of fairly consistent low level upwelling interrupted at infrequent intervals by downwelling events of such an intensity as to nearly cancel the upwelling on average. The mean actually goes negative at 21°N during August and September. These downwelling events probably reflect the occurrence of tropical storms.

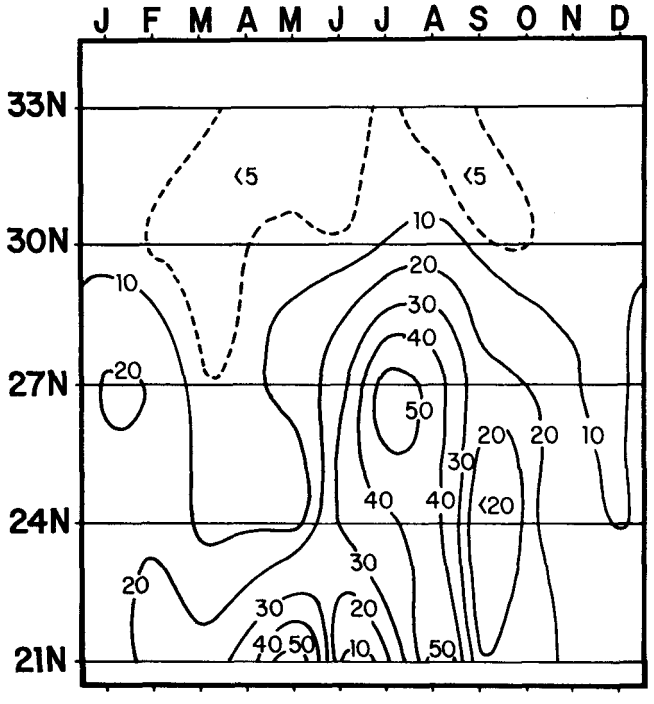

FIGURE 24. Kurtosis of monthly distributions of 6 hourly coastal upwelling indices. Locations are indicated by large dots in Figure 1. Period covered is 1967–73.

Kurtosis of the monthly distributions is greater than 3.0 at all months and locations indicating larger contributions from extreme events than would be the case in a Gaussian process (Figure 24). Off central and southern Baja California during spring and summer the large variance corresponds to large kurtosis, again indicating the importance of rare, very intense events. In the north the spring and fall seasons of maximum variance are characterized by minimum kurtosis, indicating the variance to be dominated by more frequent, less extreme pulsations.

Power spectra (Figure 25) were selected as being representative of a number of similar spectra computed for various segments of the 7 year series of 6 hourly indices. The major features, i.e., the strong diurnal peak and a general increase in energy at low

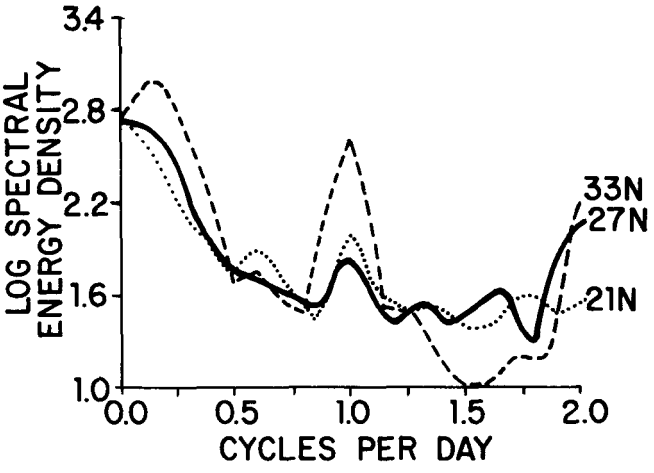

FIGURE 25. Power spectra of 6 hourly coastal upwelling indices. Spectra are plotted for time series at three locations (21°N, 107°W; 27°N, 116°W; 33°N, 119°W) for the period February 27 through July 1, 1972.

frequencies representing seasonal and other long term variations, appear consistently. The indication of a major amount of energy spread over an "event scale" of periods ranging from 2 or 3 days to several weeks is also typical. The spectral peak at the semidurnal frequency reflects the non-sinusoidal shape of the diurnal fluctuation which tends to have a faster rate of change during the morning to afternoon increase than during the evening to morning relaxation.

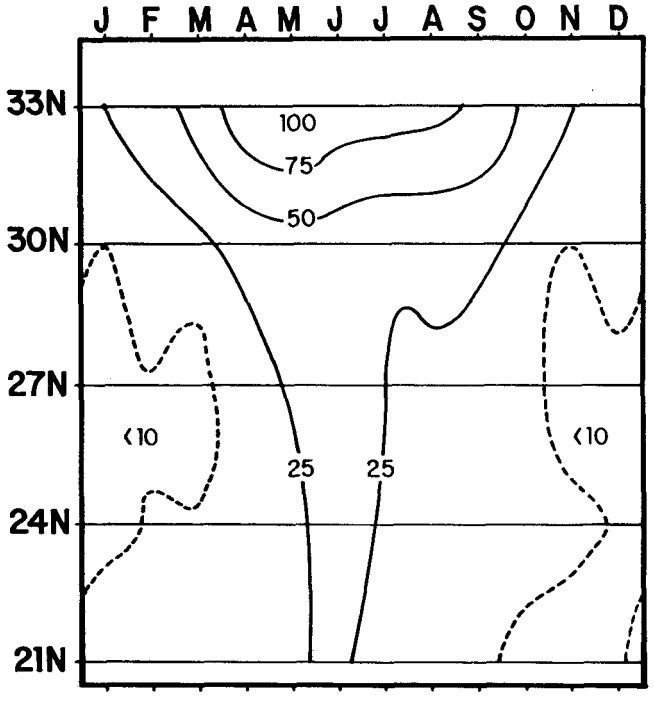

FIGURE 26. Diurnal variation in upwelling indices. Mean differences between upwelling indices computed from the 4 PM Pacific Standard Time synoptic sampling and those computed from the 10 AM sampling 6 hours earlier were computed by month at locations indicated by large dots in Figure 1. These two sampling periods tend to be extremes of the diurnal cycle as resolved by these data. Units are m^3 per second per 100 m of coast. Period covered is 1967–73.

The 10AM and 4PM (Pacific Standard Time) synoptic periods tend to be the extremes of the diurnal cycle as well as it can be resolved with the four samples per day available. The mean difference, the afternoon value minus the morning value, is positive at all months and locations (Figure 26). The amplitude tends to be greatest in the late spring and early summer and least in the winter. At 21°N latitude the minimum is earlier than at the locations further north, occuring during the fall. The diurnal variation is greatest at 33°N and is progressively smaller to the south. How much of this apparent north-south gradient in the diurnal effect may be due to the previously mentioned spatial distortion is presently unclear.

The diurnal effect is very apparent in autocorrelation functions produced from upwelling index time series (Figure 27), where the diurnal rise and fall appears superimposed on a strong decline in autocorrelation which occurs within 1 to 2 days. This rapid decline illustrates the characteristically short time scales of the indicated pulses of upwelling producing wind stress.

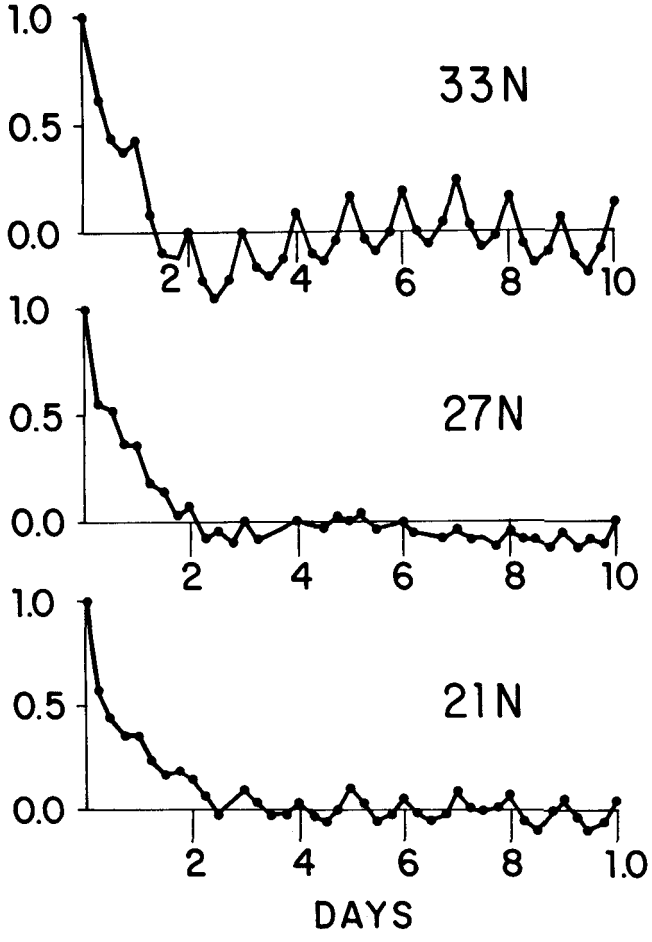

FIGURE 27. Autocorrelation functions for 6 hourly coastal upwelling indices. Functions are plotted for three locations (21°N, 107°W; 27°N, 116°W; 33°N, 119°W) during the period February 27 through July 1, 1972.

Persistence

Characteristic time scales were further examined in terms of persistence of anomalies in the 6 hourly upwelling indices (Figure 28). Since anomalies in these series tend to be much larger than the differences between various types of fits to the annual cycle, mean seasonal values were simply defined by linear interpolation between succeeding months, the midpoints of which were assigned the 7 year composite mean monthly value of the 6 hour upwelling indices. To avoid complicating effects of the diurnal cycle the analysis was done in terms of daily means. An anomaly was defined as the difference between a daily mean value and the value for the particular day from the linearly interpolated mean annual cycle. The percentage of times during the 7 year time series that a daily anomaly had the same sign as the anomaly for the previous day was computed for each month and location (Figure 28A). Situations where the anomaly was so small that it was not significantly either positive or negative were rejected by requiring the previous anomaly to have an absolute value of at least 10 m^3 per second per 100 m of coastline for the particular day to be used in the computation. This process was repeated using the respective anomalies 2, 3, and 5 days earlier in the comparisons (Figure 28B, C, and D).

The daily anomaly has the same sign as the previous day's anomaly about 70 to 80% of the time depending on month and location (Figure 28A). By the second day (Figure 28B) the persistence of sign has dropped below 50%, indicating no tendency for persistence, at some months and locations. After 5 days, the months and locations where the anomaly is below 50% are considerably greater in number than those where it is greater than 60%. Thus any persistence of individual wind stress events on scales greater than 5 days appears to be slight.

In examining these series, however, one notices a certain persistence on longer scales which is evident in groupings of individual events resulting in general levels of average intensity above or below the seasonal norm. To illustrate this a similar analysis was performed on monthly anomalies. In order to have access to a longer data series for such a monthly analysis we have used a series computed from monthly mean pressure fields which extends back to 1946. Bakun (1973) has shown that indices computed in this manner correlate highly with corresponding series of monthly means of 6 hourly indices. In order to have a value 5 months previous to our first data point for comparison, we begin with June, 1946, and then work through the following 28 years ending May, 1974. The resulting distributions (Figure 29) are somewhat more noisy than those produced from the daily series (Figure 28) because there are only 28 data points for each month and location compared to the 200 or more data points per month and location in the 7 year daily series. A level of persistence of

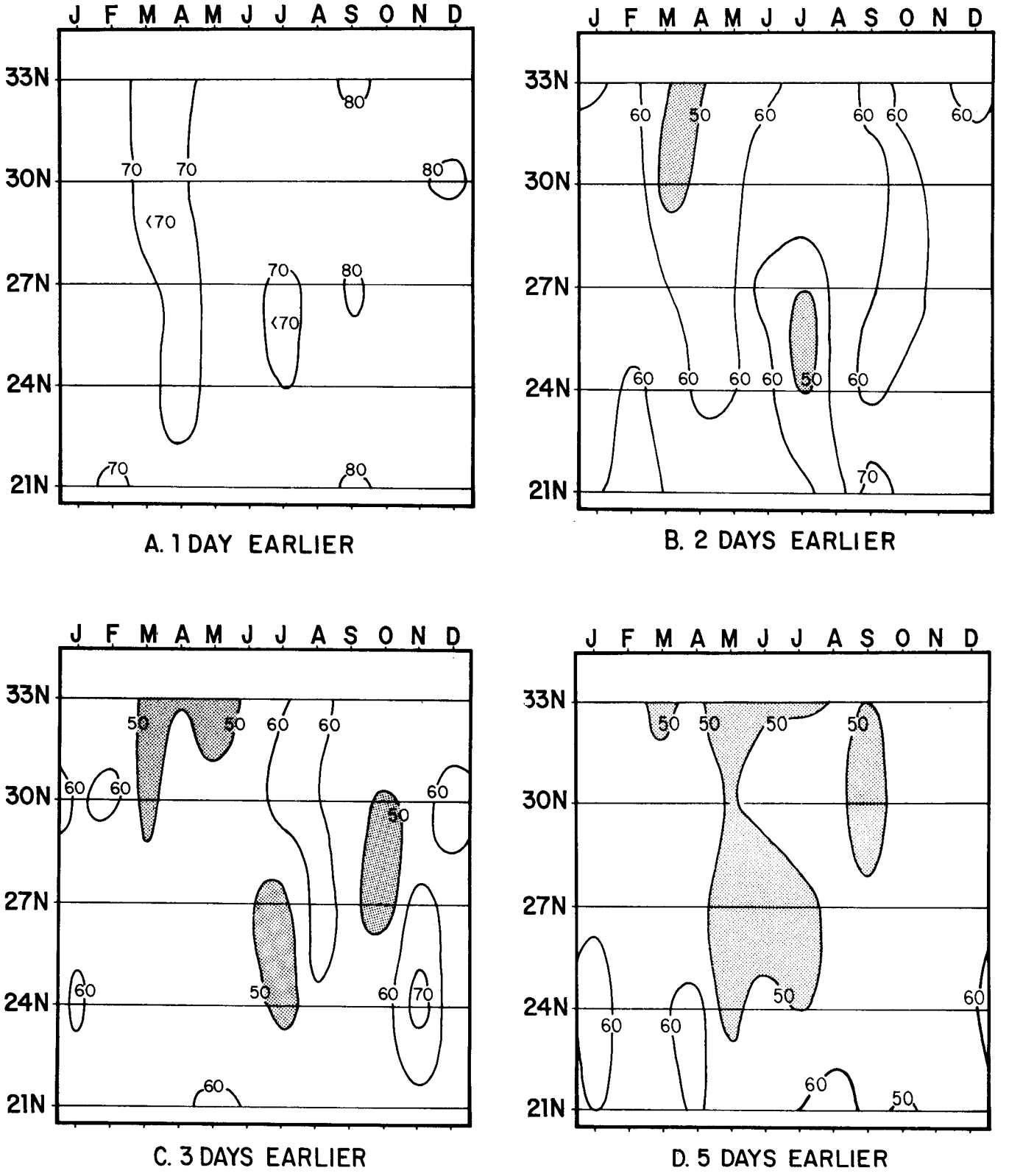

FIGURE 28. Percentage of daily upwelling index anomalies having the same sign as the daily anomaly. A. 1 day earlier, B. 2 days earlier, C. 3 days earlier, D. 5 days earlier. A daily anomaly is defined as the difference between the daily average of 6 hourly coastal upwelling indices and the characteristic value for that day derived from the long term mean annual cycle. Period covered is 1967–73. Shading indicates percentages less than fifty.

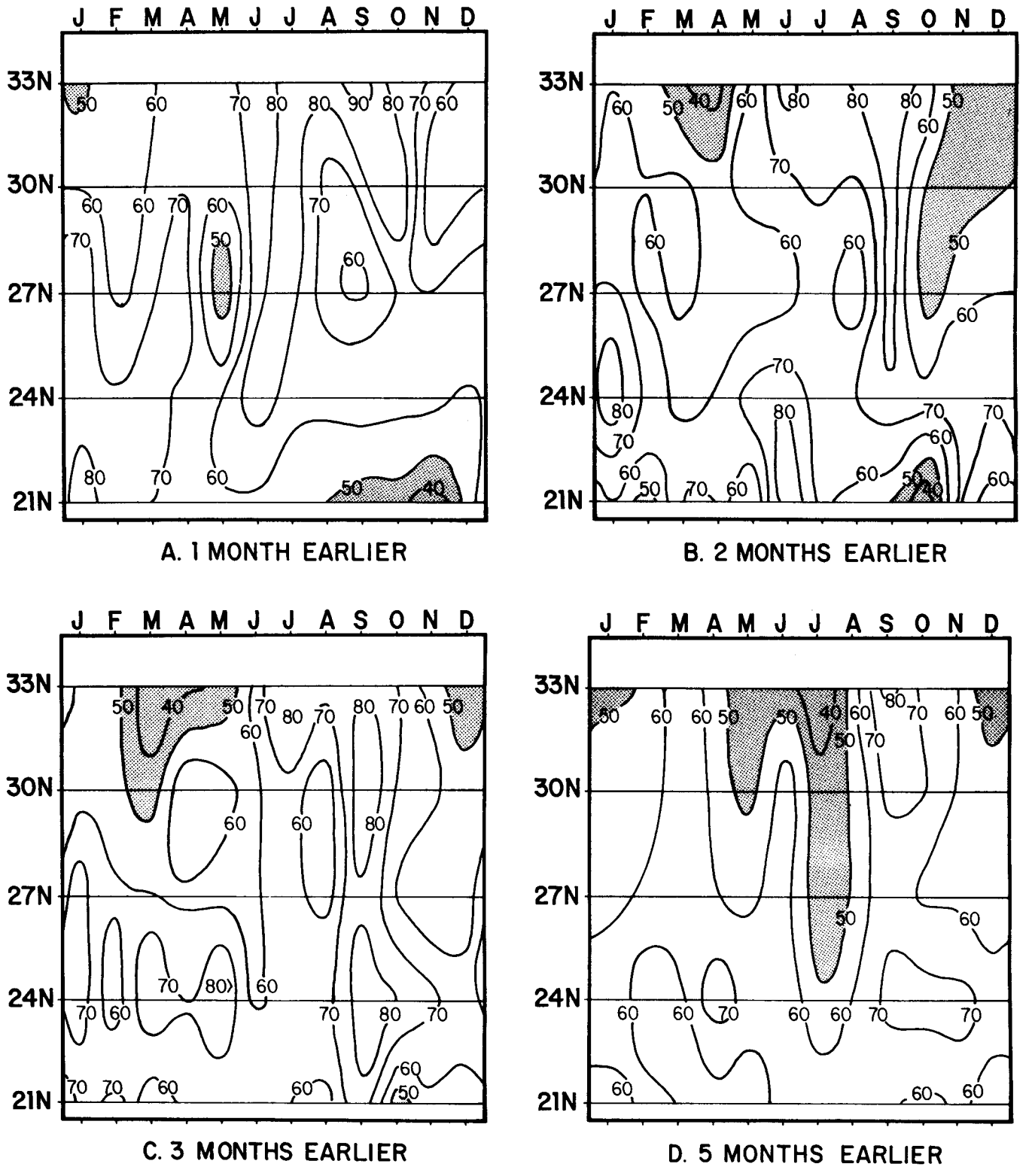

FIGURE 29. Percentage of monthly upwelling index anomalies having the same sign as the monthly anomaly, A. 1 month earlier, B. 2 months earlier, C. 3 months earlier, D. 5 months earlier. A monthly anomaly is defined as the difference between a monthly upwelling index value and a 20 year (1948–1967) mean value for the particular month. Period covered is June, 1946 through May, 1974. Shading indicates percentages less than fifty.

monthly anomalies after 5 months (Figure 29D) roughly equivalent to that for daily anomalies after 5 days (Figure 28D) is indicated.

One simple feedback system which may contribute to persistence of levels of upwelling intensity beyond the duration of individual upwelling events is as follows. An upwelling event or combination of events is eventually reflected in cooler water at the sea surface. This increases the temperature gradient in the lower atmosphere between the continent and the ocean, which in turn increases the onshore-offshore atmospheric pressure gradient. The result is greater longshore wind stress which feeds back to the upwelling process, transmitting an underlying level of intensity from one event to another. Whatever the major mechanism may be, these results suggest that general levels of upwelling intensity above or below the seasonal norm have a tendency to be persistent over periods approaching the seasonal time scale.

Spatial Coherence

Finally, an analysis using a spatial lag rather than a temporal lag, can yield some insight into the spatial coherence of upwelling anomalies. The percentage, by month and location, of daily anomalies having the same sign as the corresponding daily anomaly at 27°N latitude was determined (Figure 30). Again, we have required that the anomaly at 27°N be at least 10 $m^3/sec/100$ m of coast for it to be considered significant. The percentage at 27°N is of course always 100%. The percentage drops off more rapidly to the south than to the north. In fact at 21°N latitude it actually drops below 50% during September indicating the anomaly had a sign opposite to that at 27°N more often than not. In total, the indication is that coherence of upwelling anomalies over regions the size of the coast of Baja California is not necessarily to be expected.

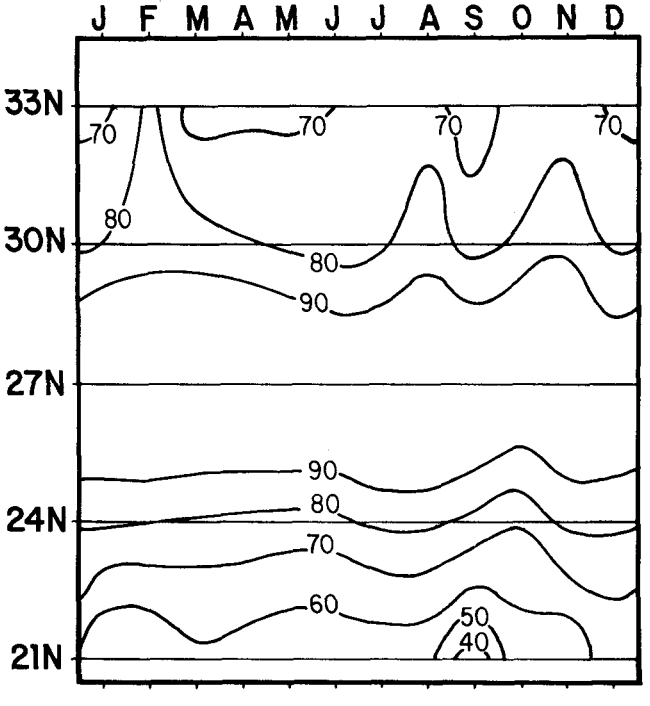

FIGURE 30. Percentage of daily upwelling index anomalies having the same sign as the corresponding daily anomaly at 27°N. Period covered is 1967–73. Shading indicates percentages less than fifty.

UPWELLING OFF BAJA CALIFORNIA DURING RECENT YEARS

We now attempt to characterize the upwelling situation off Baja California since 1972. Bakun (1973) presented coastal upwelling indices based on monthly mean data for the period 1946 through 1971. These are intended to represent the primary coastal divergence mechanism (Figure 2). These series were updated through July 1977 (Table 1) at 5 locations off southern California and northern Mexico (Figure 1). In computing these monthly indices a higher drag coefficient, 0.0026, was employed to roughly compensate for the underestimate of the stress caused by using mean data in the nonlinear calculation involved in equation (1).

In the section on the seasonal cycles we described the effect of the curl of the wind stress in causing convergence or divergence in the surface layer outside of the immediate coastal upwelling zone (Figure 19). This effect is probably important biologically. For example, certain organisms may be favored by a situation where the surface layer continues to diverge, on average, offshore of the coastal upwelling zone. Nutrients would continue to be fed into the surface layer, planktonic grazers swept away, etc. Other organisms may depend on concentration in convergent frontal zones of the organic material produced as a result of the upwelling near the coast. These might be favored by strong coastal upwelling in conjunction with or followed by strong offshore convergence.

In order to have an indicator of this effect, a set of indices of divergence of the Ekman transport field outside of the immediate coastal upwelling region was generated for the same locations and from the same monthly mean pressure fields as were the

monthly coastal upwelling indices. The applicable equation is derived by Fofonoff (1963):

$$\nabla \cdot \vec{V}_E = \frac{1}{f}(\nabla \chi \vec{\tau}) \cdot \vec{k} - \frac{\beta}{f}\vec{V}_E \cdot \vec{j} \qquad (3)$$

where:

$\nabla \cdot \vec{V}_E$	represents the divergence of Ekman transport
$(\nabla \times \vec{\tau}) \cdot \chi$	represents the vertical component of the curl of the wind stress
f	is the Coriolis parameter
β	is the meridional derivative of f,
$\vec{V}_E \cdot \vec{j}$	is the meridional component of Ekman transport.

The stress and Ekman transport inputs to equation (3) were computed as for the monthly mean upwelling indices. Numerical values were assigned as vertical velocities required to balance the computed divergences (Table 2).

During the early months of 1972, coastal upwelling appears to have been generally stronger than normal (Figure 31). This was accompanied by anomalous offshore convergence except in the extreme south where anomalous offshore divergence tends to be a persistent feature (Figure 32). Late summer and early fall of 1972 are characterized by lower than normal coastal upwelling index values except during September in the southern portion of the region. The month of December shows stronger than normal upwelling index values along the whole coast. An anomalously divergent situation is indicated offshore during November and December.

TABLE 1

Monthly coastal upwelling indices *

	JAN	FEB	MAR	APR	MAY	JUN	JUL	AUG	SEP	OCT	NOV	DEC
					1972							
33N	8	33	168	228	243	283	254	201	144	36	16	24
30N	91	88	186	180	165	168	125	113	90	61	67	85
27N	120	138	199	236	197	162	101	58	94	64	77	81
24N	85	77	161	197	179	156	53	12	84	24	59	45
21N	86	86	128	117	74	97	5	−1	13	1	38	26
					1973							
33N	15	1	182	216	290	282	288	234	167	65	75	24
30N	65	7	178	193	155	178	137	149	121	90	93	97
27N	105	28	173	181	148	138	90	115	138	106	117	97
24N	68	34	155	142	142	107	55	83	122	84	106	72
21N	39	52	163	116	108	83	16	10	27	8	19	33
					1974							
33N	1	43	91	207	372	330	229	245	159	97	26	4
30N	22	104	93	234	284	263	147	167	141	104	74	34
27N	56	105	123	208	208	160	67	116	94	80	60	39
24N	52	78	100	138	147	82	24	50	53	54	43	57
20N	31	60	81	53	125	22	4	1	4	−1	5	37
					1975							
33N	10	45	123	197	282	362	322	251	166	100	55	16
30N	50	62	127	174	187	197	192	194	180	146	134	58
27N	43	84	127	183	165	161	99	115	117	133	99	40
24N	45	85	133	185	130	93	37	46	50	96	56	35
21N	19	47	41	75	100	28	2	−1	−8	6	28	26
					1976							
33N	−1	34	120	198	304	262	277	212	88	50	4	−6
30N	44	64	139	160	231	199	160	145	70	80	54	28
27N	27	51	127	158	215	214	142	170	57	58	28	17
24N	24	50	127	153	191	172	107	86	57	72	34	32
21N	21	33	122	125	119	36	30	4	1	16	18	35
					1977							
33N	9	57	163	207	224	325	285					
30N	38	131	201	169	182	222	181					
27N	10	110	189	206	224	252	135					
24N	23	96	153	194	184	163	79					
21N	83	92	230	192	260	134	70					

* Units are cubic meters per second per 100 m length of coast. Values signify volume transported offshore in the surface Ekman layer.

TABLE 2

Monthly Surface Layer Divergence Indices*

	JAN	FEB	MAR	APR	MAY	JUN	JUL	AUG	SEP	OCT	NOV	DEC
					1972							
33N	280	15	242	-195	-328	-465	-689	-155	-218	-31	204	211
30N	97	-326	-434	-627	-651	-801	-687	-458	-408	-154	96	76
27N	-240	-236	-584	-88	-217	-232	-157	-82	-168	42	-1	82
24N	-197	-126	-255	-167	-310	-112	-10	-43	3	-24	-19	5
21N	471	354	380	321	371	303	97	9	138	29	172	87
					1973							
33N	68	-9	267	100	-367	-130	-231	-73	-45	126	119	260
30N	-6	-23	-299	-461	-892	-924	-770	-652	-726	-338	-359	63
27N	-31	-63	-165	-186	-225	-220	-239	-157	-208	-52	-124	90
24N	27	-97	-181	-189	-265	-236	-177	-62	65	22	-23	12
21N	36	152	-43	32	88	163	1	119	133	90	155	195
					1974							
33N	25	375	-103	187	-387	-651	-334	-506	-81	-69	241	310
30N	-22	18	-338	-591	-969	-903	-590	-907	-556	-385	3	151
27N	-67	-49	-118	-136	-207	-135	-45	-112	61	114	116	-65
24N	-8	-81	-121	-103	-203	-131	33	-66	30	-23	-20	-138
21N	141	135	-43	103	25	126	7	-6	88	69	140	274
					1975							
33N	390	30	-9	-65	-387	-1116	-709	-651	-73	129	416	312
33N	189	-204	-332	-503	-909	-1223	-741	-832	-535	-379	46	71
27N	-10	-65	-106	-200	-256	-350	-309	-149	-28	-45	111	15
24N	-111	-127	-160	-91	-166	-163	-163	-88	-64	-94	-37	-40
21N	97	150	135	119	13	20	-13	8	91	131	245	186
					1976							
33N	393	206	376	-64	-201	-277	-350	-570	-30	123	246	230
30N	128	-52	-180	-643	-1097	-1021	-1009	-975	-345	-155	110	111
27N	25	-26	-192	-169	-227	-311	-332	-279	-40	71	142	41
24N	-93	-55	-144	-4	-155	210	-4	41	64	-64	-44	-83
21N	223	215	486	573	553	389	368	128	109	357	413	489
					1977							
33N	230	315	317	-111	-160	-827	-493					
30N	98	-12	-470	-787	-982	-1557	-1155					
27N	72	157	-75	-416	-449	-681	-269					
24N	-137	-5	-217	-409	-218	-131	-27					
21N	668	719	289	382	-312	95	228					

*Values signify vertical velocities at the bottom of the Ekman layer required to balance the indicated divergence or convergence occurring offshore of the primary coastal upwelling zone. Units are millimeters per day, positive upwards.

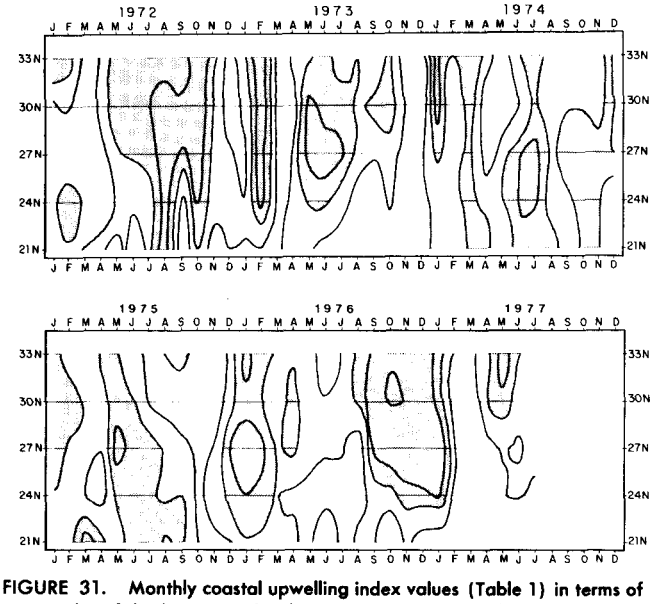

FIGURE 31. Monthly coastal upwelling index values (Table 1) in terms of quartiles of the frequency distribution made up of all values for the given location and calendar month within the 1946–77 time series. Quartiles are delineated by contours. The two quartiles below the median are shaded.

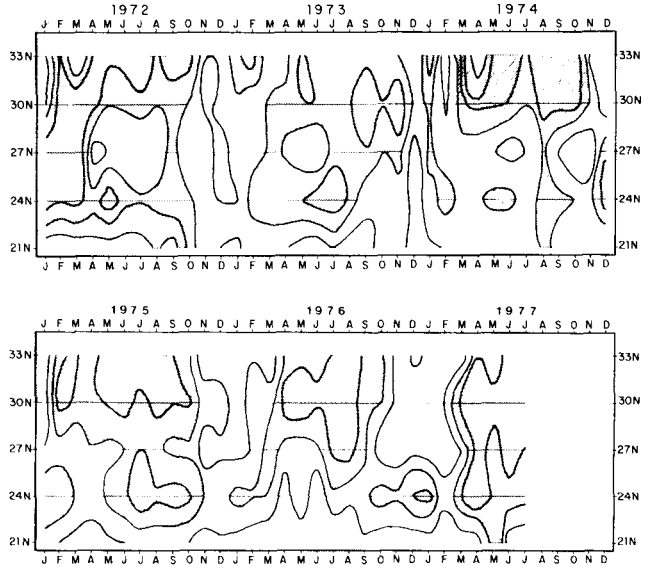

FIGURE 32. Monthly offshore surface layer divergence indices (Table 2) in terms of quartiles of the frequency distribution made up of all values for the given location and calendar month within the 1946–77 time series. Quartiles are delineated by contours. The two quartiles below the median are shaded.

Weak coastal upwelling is indicated off Baja California in February followed by higher than normal intensity during March and April (Figure 31). In the north a low tendency prevailed from May through October coupled with greater than normal offshore convergence. At 21°N latitude the coastal upwelling indices were anomalously high all year, becoming extremely anomalous late in the year. Extreme values appear all along the coast during November and December. The indication of high offshore divergence which is a persistent feature at 21°N during the recent period spreads northward along the whole coast during December (Figure 32).

An alternating pattern off northern Baja California was evident during early 1974 with a low upwelling index anomaly in January, a high anomaly in February, a low in March, and very high values in April and May. Low values appear in the south central region during June and July. The northern area is characterized by anomalous offshore convergence from May through October.

Generally higher than normal coastal upwelling is indicated during March 1975, followed by a period of lower than normal intensity which lasts until May in the north, but continues generally through the summer in the south. The latter portion of 1975 exhibits higher than normal coastal upwelling index values. The offshore region appears to have been anomalously convergent, particularly during summer and early fall (Figure 32).

A period of weak coastal upwelling is indicated during early 1976, followed by stronger than normal upwelling during the summer. The fall and winter are characterized by lower than normal upwelling index values as far south as 24°N latitude. The offshore divergence index values indicate anomalous convergence in the north during spring and summer of 1976, and anomalous divergence during late fall.

During the final revision of this paper, index values were available for the first 7 months of 1977. Coastal upwelling index values are generally above average except during January and during May in the north (Figure 31). Offshore divergence index values are high during January and February, but anomalously low during spring and early summer (Figure 32).

Offshore divergence index values at 21°N tend to be very high in this recent 6 year period relative to the values in earlier years of the time series (Figure 32). Whether this reflects a real longer period variation in the wind pattern is not clear at this time. Changes in the distribution of available data or in the meteorological analysis procedures may be affecting the computed values. In general, care should be exercised in attempting to discern long term trends using this type of index series. Rather, the purpose is to provide a useful indication of relative variations within groups of fairly contemporaneous years.

CONCLUDING REMARKS

In our descriptions of seasonal features, the summaries by 1 degree squares indicated significant spatial variations on scales smaller than the 3 degree resolution we can achieve in synoptic indices. Relating the large scale indices to smaller scale features may require the "engineering approach" suggested by Smith (1968) where one looks at the "outputs," in our case physical or biological data on a smaller scale in those particular instances where it is available from research cruises, shore stations; etc., and the larger scale synoptic "inputs" and attempts to define the "transfer functions." As a first approximation it may be reasonable to assume, for example, that where greater than normal convergence is indicated on the larger scale, smaller scale divergences which exist might weaken and convergences strengthen.

We are continuing to assemble pertinent data including ocean-atmosphere heat exchange components, dynamic topographies from hydrographic data, sea level records, mixed layer depths, temperature series from shore stations, river runoff records, etc. We are looking into possibilities of satellite inputs and are in the process of expanding our wind stress indices to lower latitudes using newly developed "global band" atmospheric products (Lewis and Grayson, 1972).

Our plans for the future include computer modelling of some of the processes controlling the fishery environment. It is sometimes the case in fishery oceanography that rather than having too little detail in our environmental descriptions we have too much, and very little means to integrate it into a total "environmental condition" which will make sense in terms of a total fishery. Modelling, rather than creating any new data, may help to distill the various data available down to a useable number of significant factors, the year to year variations of which could be quantitatively compared. Time series of these factors might be generated from historical data and related to the past history of fishery stocks. Continuous operational updates could than perhaps provide practical environmental inputs for systems approaches to fishery management.

REFERENCES

Bakun, Andrew. 1973. Coastal upwelling indices, west coast of North America, 1946–71. NOAA Tech. Rep. NMFS SSRF-671, 103 pp.

——— 1975. Daily and weekly upwelling indices, west coast of North America, 1967–73. NOAA Tech. Rep. NMFS SSRF-693, 115 pp.

Bakun, Andrew, Douglas R. McLain, and Frank V. Mayo. 1974. The mean annual cycle of coastal upwelling off western North America as observed from surface measurements. Fish. Bull. U.S., 72 (3): 843–844.

California Marine Research Committee. 1963. CalCOFI atlas of 10-meter temperatures and salinities 1949 through 1959. CalCOFI Atlas, (1).

Davidson, Kenneth L. 1974. Observational results on the influence of stability and wind-wave coupling on momentum transfer and turbulent fluctuations over ocean waves. Boundary-Layer Met., 6: 305–331.

Denman, Kenneth L., and M. Miyake. 1973. Behavior of the mean wind, the drag coefficient, and the wave field in the open ocean. J. of Geophys. Res., 78: 1917–1931.

Ekman, V. Walfrid. 1905. On the influence of the Earth's rotation on ocean currents. Arkiv. Math. Astros. Fysik., 2 (11): 1–55.

Fofonoff, Nicholas P. 1962. Dynamics of Ocean Currents. *In,* The Sea, M.N. Hill, ed., Interscience Pub., New York, 1: 323–395.

Holl, Manfred, and Bruce R. Mendenhall. 1972. Fields by information blending: Sea-level pressure version. FNWC Tech. Note, (72-2): 1–65.

Huyer, Adriana, Barbara M. Hickey, J. Dungan Smith, Robert L. Smith, and R. Dale Pillsbury. 1974. Coherence at low frequencies in currents observed over the continental shelf off Oregon and Washington. (Abstract) (0–36), EOS-Trans. Am. Geophys. Union, 55 (12): 1135.

Lewis, John M., and Thomas H. Grayson. 1972. The adjustment of surface wind and pressure by Sasaki's variational matching technique. FNWC Tech. Note, 72-1: 1–49.

Lynn, Ronald L. 1967. Seasonal variation of temperature and salinity at 10 meters in the California Current. Calif. Coop. Oceanic Fish Invest., Rept. 11: 157–186.

Munk, Walter H. 1950. On the wind driven ocean circulation. J. Met., 7 (2): 79–93.

Pedlosky, Joseph. 1974. Longshore currents, upwelling and bottom topography. J. of Phys. Oceanogr., 4, 214–226.

Reid, Joseph L., Jr., Gunnar I. Roden, and John G. Wyllie. 1958. Studies of the California Current system. Calif. Coop. Oceanic Fish. Invest., Prog. Rept., 1 July 1956 to 1 January 1958: 27–57.

Robinson, Margaret K. and Roger A. Bauer. 1971. Atlas of monthly mean sea surface and subsurface temperature and depth of the top of the thermocline, North Pacific Ocean. FNWC, Monterey, California.

Seckel, Gunter, R., and Frederick H. Beaudry. 1973. The radiation from sun and sky over the North Pacific Ocean. (Abstract) (0–33), EOS-Trans. Am. Geophys. Union, 54 (12): 1114.

Smith, Robert L. 1968. Upwelling. Oceanogr. Mar. Biol. Ann. Rev., 6: 11–46.

Stidd, Charles K. 1974. (Abstract) (O–1), EOS-Trans. Am. Geophys. Union, 55 (12): 1132.

Sverdrup, Harald U., Martin W. Johnson, and Richard H. Fleming. 1942. The oceans; their physics, chemistry, and general biology. Prentice-Hall, New York, 1087 p.

Wooster, Warren S., and Joseph L. Reid, Jr. 1963. Eastern Boundary Currents. *In,* The Sea. M. N. Hill, ed., Interscience Pub., New York, 2: 253–280.

Wyllie, John G., and Ronald J. Lynn. 1971. Distribution of temperature and salinity at 10 meters, 1960–1969, and mean temperature, salinity and oxygen at 150 meters, 1950–1968,. in the California Current. Calif. Coop. Oceanic. Invest., Atlas, (15): 1–188.

Wyrtki, Klaus. 1965. Surface currents of the eastern tropical Pacific Ocean. Inter-Amer. Trop. Tuna Com., Bull., 9 (5): 271–304.